AD-A111 787 VIRGINIA POLYTECHNIC INST AND STATE UNIV BLACKSBURG --ETC F/G 20/4
PARABOLIZED NAVIER-STOKES PREDICTIONS FOR THREE-DIMENSIONAL VIS--ETC(U)
MAY 81 S SWAMINATHAN, M D KIM, R A THOMPSON

UNCLASSIFIED NL

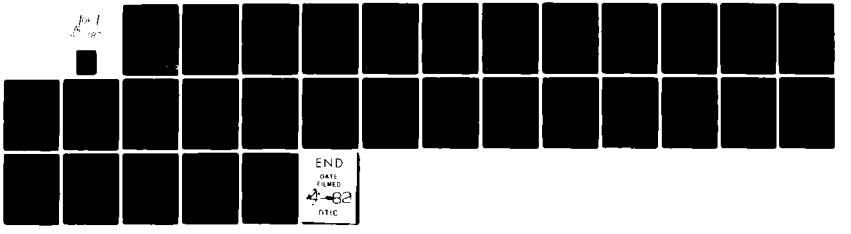

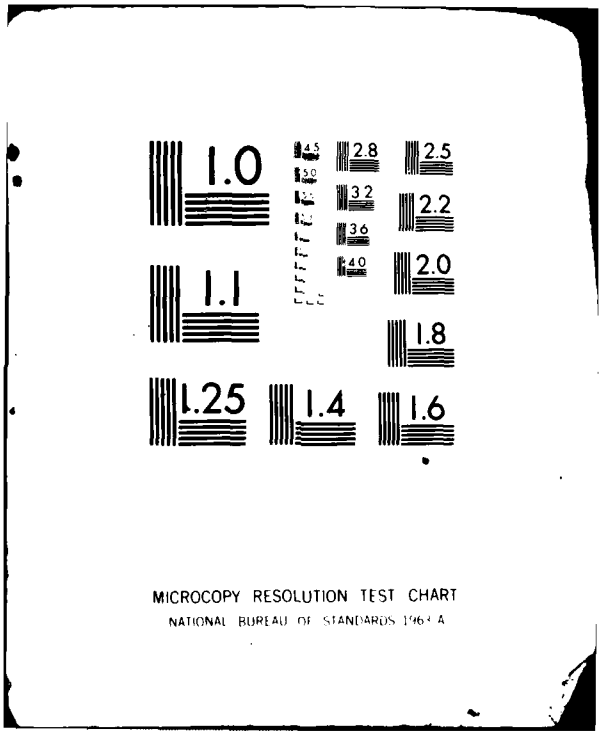
1.0
1.1
1.25
1.4
1.6
1.8
2.0
2.2
2.5
2.8
3.2
3.6
4.0
4.5
5.0
MICROCOPY RESOLUTION TEST CHART
NATIONAL BUREAU OF STANDARDS 1963 A

PARABOLIZED NAVIER-STOKES PREDICTIONS FOR THREE-DIMENSIONAL VISCOUS SUPERSONIC FLOWS

S. Swaminathan,* M. D. Kim,*

R. A. Thompson,** and C. H. Lewis†

Virginia Polytechnic Institute and State University
Aerospace and Ocean Engineering Department
Blacksburg, Virginia

14 MAY 81

ABSTRACT

A parabolized Navier-Stokes Code (HYTAC) is used to predict the supersonic, laminar or turbulent viscous flow about arbitrary geometries at moderate angles of attack, and the results are compared with those from other viscous and inviscid codes. The test cases presented in this paper include the external flow over a supersonic, blunt nosed inlet, a slab delta wing and an elliptic body at various Mach numbers. The results for the inlet are compared with the results from a viscous shock-layer code (VSL3D) and they show good agreement. The slab delta wing surface pressure compares well with the results from an inviscid code (STEIN) and with experimental results. The surface heat transfer for this case is in good agreement with the results from a boundary layer code using streamline tracing (TRACE) and with experimental results.

INTRODUCTION

The design and successful flight of high speed inlets and complex lifting and reentry vehicles can be aided by the use of accurate and efficient computational fluid dynamics. In this paper, results of computer analyses of three bodies of complex shapes are given. The first body considered is a supersonic blunt nosed inlet, designed to operate at Mach numbers from 4 to 7 and at angles of attack up to 10 degrees (Figure 1). The inlet is a sphere-cone with an afterbody of smooth curvature. The second body is a slab delta wing with 80 degree sweep angle (Figure 2). This wing has a nose radius of 0.5 inch and is designed to operate at a Mach number of 9.6 at various angles of attack. The third geometry is an elliptic body, which has a spherical nose of 0.3 feet radius and an afterbody with elliptical cross section (Figure 3). The change from spherical to elliptical cross section is gradual, and the final cross section of 2:3 ellipse is achieved within 8 to 10 nose radii. This body is designed to operate at Mach numbers of about 20. Flight

*Graduate Student
**Senior Undergraduate Student
†Professor

performance under all the above conditions requires a thorough understanding of the aerodynamic forces and the surface heat transfer and of their influence on the vehicle trajectory and structure.

The flowfield over such general bodies can be quite complicated. The blunt nose generates a bow shock and within the shock layer, depending on the body geometry, imbedded shocks and expansion waves may exist. At moderate angles of attack there could be a large region of crossflow separation. The flowfield over these bodies under such flow conditions can be numerically predicted by solving the steady, three-dimensional Parabolized Navier-Stokes (PNS) equations. This method has a great savings in computer time compared to the solution of full Navier-Stokes equations. The PNS equations are parabolic in the streamwise direction and elliptic in the crossflow direction which makes it possible for this method to solve the crossflow separated region. The derivatives are written in the conservative form which makes it possible to capture the imbedded shocks in the flowfield.

In recent years the three-dimensional viscous shock-layer approach (VSL3D)[1] and the Parabolized Navier Stokes method (PNS)[2-4] have been applied to various problems. The VSL3D equations are parabolic in both streamwise and crossflow directions and are solved by efficient methods which require substantially less computing time than the PNS method. The VSL3D[1] method can be applied to general geometries to obtain the flowfield solution over the entire body when the angle of attack is not too high. For high angles of attack, the PNS methods are more efficient in handling crossflow separation.

In this paper, the general bodies noted above have been analyzed by different methods and the results are compared. The HYTAC code, developed by Helliwell and coworkers,[4,5] has been used to analyze all three bodies. The inlet has been analyzed by HYTAC, and the results are compared with those from VSL3D[1] . The results for the slab delta wing are compared with those from an inviscid plus streamline heat-transfer code (BLUNT STEIN-TRACE)[6-9] and experimental results.[10]

The HYTAC code uses a body-normal, shock-normal nonorthogonal coordinate system (Figure 4). In this coordinate system the body and the bow shock are ξ-ζ coordinate surfaces. The second coordinate η is body-normal and shock-normal and always orthogonal to the ξ and ζ coordinates. At the body no-slip boundary conditions are used and the enthalpy is specified. At the shock, the freestream velocity vector is transformed into the computational coordinate direction, and then the Rankine-Hugoniot jump conditions are used. The governing equations are solved by implicit differencing in the η-ζ plane. A Gauss-Seidel iteration procedure is used in solving the equation.

ANALYSIS

Generation of a suitable computational grid is one of the important steps in the numerical solution of flowfields. In the present study, a body-oriented nonorthogonal coordinate system (ξ,η,ζ) has been used. The first coordinate, ξ is along the body in the primary flow direction (Figure 4). The third coordinate lines (ζ) are constructed to be normal to the ξ coordinate on the body surface, and this facilitates easy calculation of body forces and

moments and easy introduction of surface boundary condition. The second coordinate (η) is constructed normal to both ξ and ζ -coordinate lines in the region between the body and the shock surfaces. The shock surface is taken as a ξ-ζ coordinate surface (η=1) and the η-coordinate lines are both body-normal and shock normal. A body-oriented cylindrical coordinate system is used as the reference coordinate system for the interpretation of the body geometry, shock shape and every grid point. In this sytem, the ξ and ζ coordinates will not be orthogonal to each other in the region between the body and shock surfaces.

The steady three-dimensional parabolized Navier-Stokes equations are written in nondimensional form in a general curvilinear coordinate system. In the equations for the stress tensor components, all the derivatives with respect to ξ were neglected. The resulting equations are parabolic in the ξ coordinate direction and elliptic in the crossflow direction. The governing equations are solved by implicit differencing in the η-ζ plane. The ξ derivatives are approximated by a backward difference, while the η and ζ derivatives are written in terms of an unequally spaced three-point difference scheme. The equations were linearized by the Newton-Raphson method and subsequently solved by Gauss-Seidel iteration.

At the surface boundary, no-slip conditions are used and the enthalpy is specified. Pressure on the body surface is obtained from the v-momentum equations. At the plane of symmetry, ζ = 0 and 180 degrees, w and g_{13} are antisymmetric while all the other variables and metrics are symmetric. At the shock Rankine-Hugoniot jump conditions are used as the boundary condition. Since the shock standoff distance is also an unknown, the continuity equation is used as a sixth equation.

For a numerical procedure using a marching scheme, the construction of an accurate initial data plane is important in obtaining the correct solution of the whole flowfield. The entire flowfield, coordinate and metrics at the initial data plane have been generated using a viscous shock-layer method. The coordinate and metrics for the body-normal, shock-normal coordinate system have been generated from the two-step body-normal data of the shock-layer solution by the method described in References 4 and 5.

DESCRIPTION OF GEOMETRY AND FREESTREAM CONDITIONS

The various geometries included in this study are blunt [illegible]d supersonic inlets, an 80-deg swept slab delta wing and an elliptic body [illegible]this section the details of the geometries and the freestream conditions under which they are analyzed are explained.

The inlet is a blunt sphere-cone with an afterbody of smooth curvature. The blunt nose has a radius of 0.5 inch and the cone angle is 12.5 degrees. The afterbody is expressed in analytical form and the complete inlet is shown in Figure 1. In the present study, the external flowfield up to the cowl lip has been analyzed. The analysis of the inlet is done for a freestream Mach number of 7 at 0 and 5 degrees angles of attack. Although the program has a capability to analyze a laminar flowfield, in this case turbulent flow is assumed and a two-layer eddy-viscosity model is used. The wall temperature is assumed to be constant, and the analysis is done for two

different temperatures. The details of the freestream conditions are given in Table 1.

Surface heat-transfer and pressure distribution over an 80-deg swept slab delta wing have been studied for a Mach number of 9.6 at zero and 10 degrees angles of attack. The wing has cylindrical leading edges, and a hemispherical nose of 0.5-inch radius. The length of the body is about 15 nose radii. The details of the geometry are given in Figure 2. In this case the laminar flow regime has been considered, and the surface temperature is about 540R.

The elliptic body has a spherical nose of radius 0.3 feet and an afterbody with elliptical cross section. The change from spherical cross section to the elliptical cross section is gradual and is finally achieved after 8 to 10 nose radii. The final cross section obtained is a two by three ellipse. This body has been analyzed for a freestream Mach number of 20. The analysis is done for laminar flow and for a surface temperature of 800R. The details of the geometry are given in Figure 3, and the freestream conditions are given in Table 1.

RESULTS AND DISCUSSION

INLET GEOMETRY

Figures 5 and 6 show the variation of surface pressure and heat transfer for the inlet geometry at zero angle of attack. The surface pressure predictions agree very well with results from a viscous shock-layer code (VSL3D).[1] The surface heat-transfer predictions by HYTAC is higher than those from VSL3D by about 30 percent. Figures 7, 8 and 9 show the axial velocity, static pressure and enthalpy profiles for this case. From these profiles it can be seen that the HYTAC code is capable of capturing the imbedded shocks.

Figures 10 and 11 show the variation of surface pressure and heat transfer for angle of attack 5 degrees for various ζ angles. The solution could be obtained only up to 61 nose radii, and it was found that at this point axial separation occurred. This can be verified from the plot of axial shear stress variations as shown in Figure 12. At this point the surface slope of the body is about 20 degrees.

SLAB DELTA WING

The computed surface pressure from HYTAC and STEIN are compared with experimental results for both ζ = 0 and 90 deg (Figures 13 and 14). For both cases the results are in good agreement. Figures 15 and 16 show the comparison of surface heat-transfer results from TRACE and HYTAC with the experimental results for ζ = 0 and 90 deg. The predictions are good in the nose regions for both the cases. For the downstream region, HYTAC predicts a lower heat transfer for both cases. The predictions by TRACE seem to be in error in the far downstream region at ζ = 90 deg. This may be due to the fact that the computed streamlines diverge from leading edge.

Figures 17 and 18 show the surface pressure results from STEIN and HYTAC for α = 10 deg for both ζ = 0 and 90 degree planes. For ζ = 0, the results are compared with the experimental values, and both HYTAC and STEIN underpredict

the surface pressure. Experimental results are not available for ζ = 90 degree plane; however, the results from HYTAC and STEIN agree very well.

Figures 19 and 20 show the surface heat-transfer results from HYTAC and TRACE for α = 10 deg for both ζ = 0 and 90 degree planes. The results for the nose region agree well with the experimental values; however, both codes underpredict the surface heat transfer in the downstream region.

ELLIPTIC BODY

Figures 21 and 22 show the variation of surface pressure and heat transfer for various ζ planes for the elliptic body. Both the surface pressure and heat transfer are higher at the windward plane. Since the sphere-cone tangent locations depend on ζ, a patching is needed to obtain a smooth variation. This procedure resulted in a slightly concave region for ζ = 0 and 30 deg (Figure 31). The increase in surface pressure between s = 1.5 and 2.5 is due to this concavity in the geometry.

CONCLUDING REMARKS

The capability of HYTAC in predicting the three-dimensional viscous-supersonic flows over three geometries has been shown by comparison with experimental results and results from a viscous shock-layer code indicates that HYTAC can accurately solve the flowfield over axisymmetirc and nonaxisymmetric geometries. Although HYTAC requires more computing time, it is capable of solving the crossflow separated region. However, by looking at the results for the inlet geometry, it can be seen that HYTAC is unable to solve flowfields with axial separation. In this particular case, even though the flow is attached for zero angle of attack, at moderate angles of attack like 5 degrees, the flow separates on the leeward side. In order to solve the separated flowfields, the time dependent Navier-Stokes equations must be solved.

Comparing the results for the inlet for zero angle of attack, with those from VSL3D shows that the VSL3D is able to solve the flowfield in less time. Although the surface pressure results are in good agreement, the surface heat-transfer results from HYTAC is higher by 30 percent. Due to lack of experimental data, the computational results could not be verified.

Both HYTAC and STEIN predicted the surface pressure over the slab delta wing reasonably accurately. The results for zero angle of attack agree very well with the experimental results. Both HYTAC and STEIN underpredict the surface pressure for 10 degree angle of attack. For the nose region the surface heat-transfer results from TRACE and HYTAC agree very well with the experimental results. For the downstream region, the prediction by TRACE seems to be in error, and this is due to the fact that the computed streamlines diverge from leading edge.

The results for the elliptic body could not be compared with other results due to a lack of data. HYTAC predicts higher heat transfer and surface pressure at the windward plane. Because of the presence of a concavity in the geometry near the sphere-cone tangent point for ζ = 0 and 30 degrees, the surface pressure results are higher at these locations.

In summary, methods have been shown which can predict supersonic viscous flowfield over complex three-dimensional bodies at angles of attack up to about 15 degrees.

NOMENCLATURE

g_{ij}	coordinate metric tensor i, j = 1,2,3
H	total enthalpy, H^*/h_∞
h	static enthalpy, h^*/h_∞
M_∞	freestream Mach number
p	pressure, $p^*/\rho_\infty U_\infty^2$
P_{ref}	reference pressure, $\rho_\infty U_\infty^2$
$\dot{q}^*$	dimensional heat-transfer rate
Re_∞, R_n	freestream Reynolds number
R_n	nose radius of curvature
STINF	Stanton number, $\dot{q}^*/\rho_\infty U_\infty (H_0^* - H_w^*)$
s	surface distance coordinate measured along the body, s^*/R_n^*
T	temperature, T^*/T_∞
U_∞	dimensional freestream velocity
u	velocity component along ξ coordinate, u^*/U_∞
v	velocity component along η coordinate, v^*/U_∞
w	velocity component along ζ coordinate, w^*/U_∞
z,r,ϕ	body-oriented cylindrical coordinate system
α	angle of attack, degree
θ_c	cone half angle, degree
μ	coefficient of viscosity, μ^*/μ_∞
ρ	density, ρ^*/ρ_∞
η	coordinate, body-normal, shock-normal direction
ξ	coordinate, along the body
ζ	coordinate, normal to ξ and η on the body surface

Subscript

w	wall value
0	stagnation condition
∞	freestream condition (dimensional quantity)

Superscript

*	dimensional quantity

REFERENCES

1. Szema, K. Y. and Lewis, C. H.: "Three-Dimensional Hypersonic Laminar, Transitional and/or Turbulent Shock-Layer Flows." AIAA Paper No. 80-1457. AIAA 15th Thermophysics Conference, Snowmass, Colorado, July 14-16, 1980.

2. Lubard, S. C. and Helliwell, W. S.: "Calculation of the Flow on a Cone at High Angle of Attack," AIAA J., Vol. 12, No. 7, July 1974, pp. 965-974.

3. Agopian, K., Collins, J., Helliwell, W., Lubard, S. C. and Swan, J.: "NASA Viscous 3-D Flowfield Calculations," R&D Associates, RDA-TR-6100-007, October 1975.

4. Helliwell, S. W., Dickinson, R. P. and Lubard, S. C.: "HYTAC Phase 1 Report: Viscous Flow over Arbitrary Geometries at High Angle of Attack," Arete Associates Technical Report, AR-79-046-TR, April 24, 1979.

5. Helliwell, W. S., Dickinson, R. P. and Lubard, S. C.: "HYTAC User's Manual," Arete Associates Technical Report, AR-80-207-TR, July 31, 1980.

6. Moretti, G. and Bleich, G.: "Three-Dimensional Flow Around Blunt Bodies," AIAA J., Vol. 5, 1966.

7. Marconi, F., Salas, M. and Yaeger, L.: "Development of a Computer Code for Calculating the Steady Super/Hypersonic Inviscid Flow Around Real Configurations." Volume I - Computational Technique, NASA-CR-2675, April 1976.

8. Marconi, F., Salas, M. and Yaeger, L.: "Development of a Computer Code for Calculating the Steady Super/Hypersonic Inviscid Flow Around Real Configurations." Volume II - Code Description, NASA-CR-2676, April 1976.

9. Hamilton, H. Harris: "Calculation of Heating Rates on Three-Dimensional Configurations," thesis for Degree of Engineer, School of Engineering and Applied Science of the George Washington University, December 1978.

10. Whitehead, A. H. Jr. and Dunavant, J. C.: "A study of Pressure and Heat Transfer over an 80° Sweep Slab Delta Wing in Hypersonic Flow," NASA-TN-D2708, Langley Research Center, November 9, 1964.

TABLE I. TEST CASE CONDITIONS

Geometry	Flow Type	Nose Radius (ft)	α (deg)	M_∞	FREESTREAM CONDITIONS					WALL CONDITIONS	
					Altitude (ft)	T_∞ (^oR)	Re_{∞,R_n}	ρ_∞ (lbm/ft^3)	U_∞ (ft/sec)	T_w/T_0	T_w/T_∞
INLET	TURB	0.04167	0	7	80,000	394.69	81781.4	2.78×10^{-3}	6816.3	0.1877	2.027
INLET	TURB	0.04167	0	7	80,000	394.69	81781.4	2.78×10^{-3}	6816.3	0.821	8.867
INLET	TURB	0.04167	5	7	80,000	394.69	81781.4	2.78×10^{-3}	6816.4	0.821	8.88
ELLIPTIC	LAM	0.3	0	20		392.59	542841	4.76×10^{-3}	19423.3	0.02516	2.0378
SLAB DELTA	LAM	0.04167	0	9.6		84.4	57701.3	6.46×10^{-4}	4348.5	0.33	6.413
SLAB DELTA	LAM	0.04167	10	9.6		84.4	57701.3	6.40×10^{-4}	4348.5	0.33	6.413

TABLE II. TEST CASE COMPUTING TIMES*

	α (degrees)	Method of Solution	ξ range	ξ steps	η points	ζ planes	Time min:sec
INLET	0	HYTAC	1.22-69	137	50	3	9:20
INLET	0	VSL3D	0-69.7	135	101	1	3:44
INLET	5	HYTAC	1.14-61	96	50	19	57:47
SLAB DELTA	0	HYTAC	1.22-14.2	50	50	19	39:22
	10	HYTAC	1.22-9.64	33	50	19	27:35
ELLIPTIC	0	HYTAC	1.22-8.18	28	50	19	20:01

*CPU time on IBM 3032 H=OPT2 compiler.

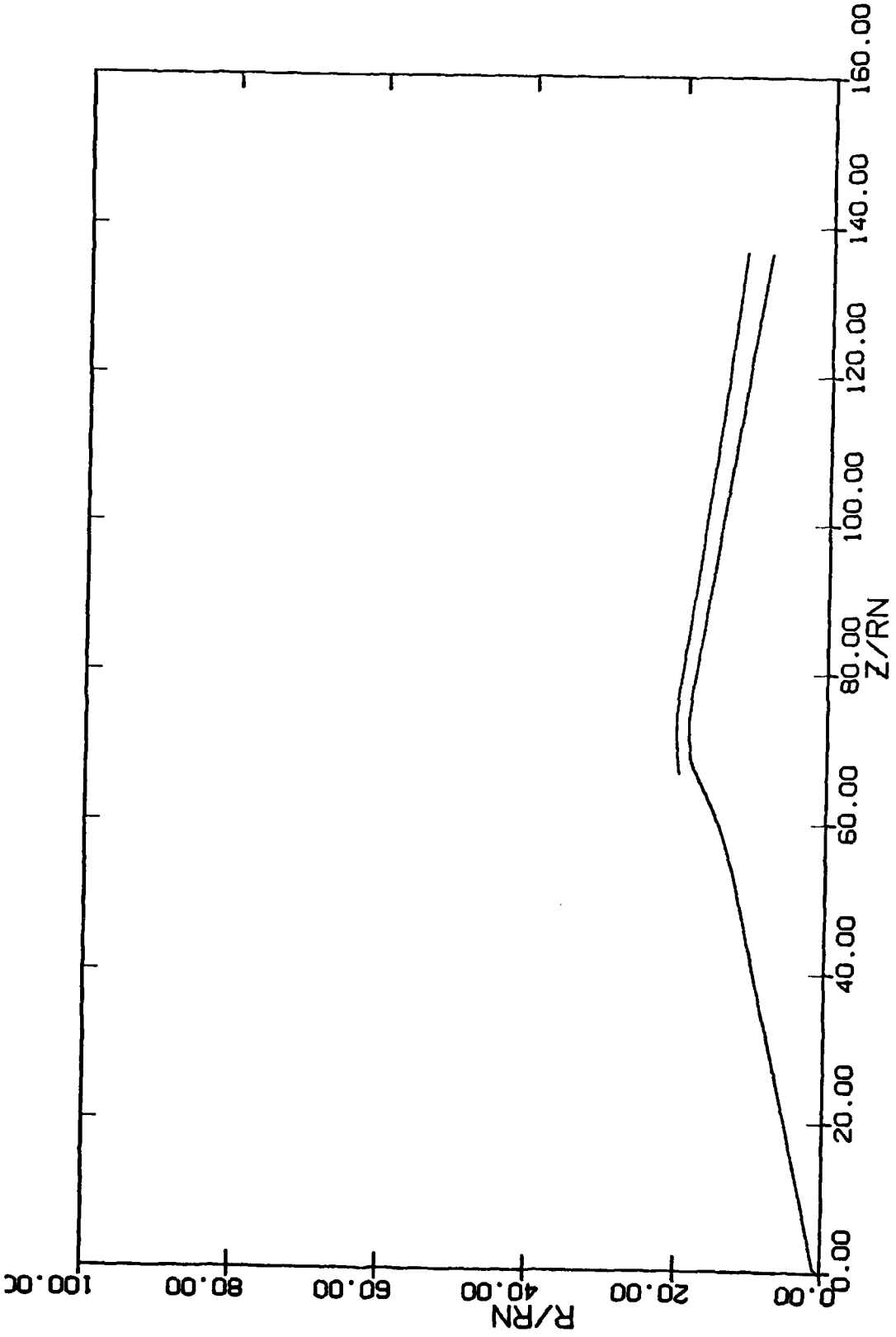

Figure 1. Inlet Geometry

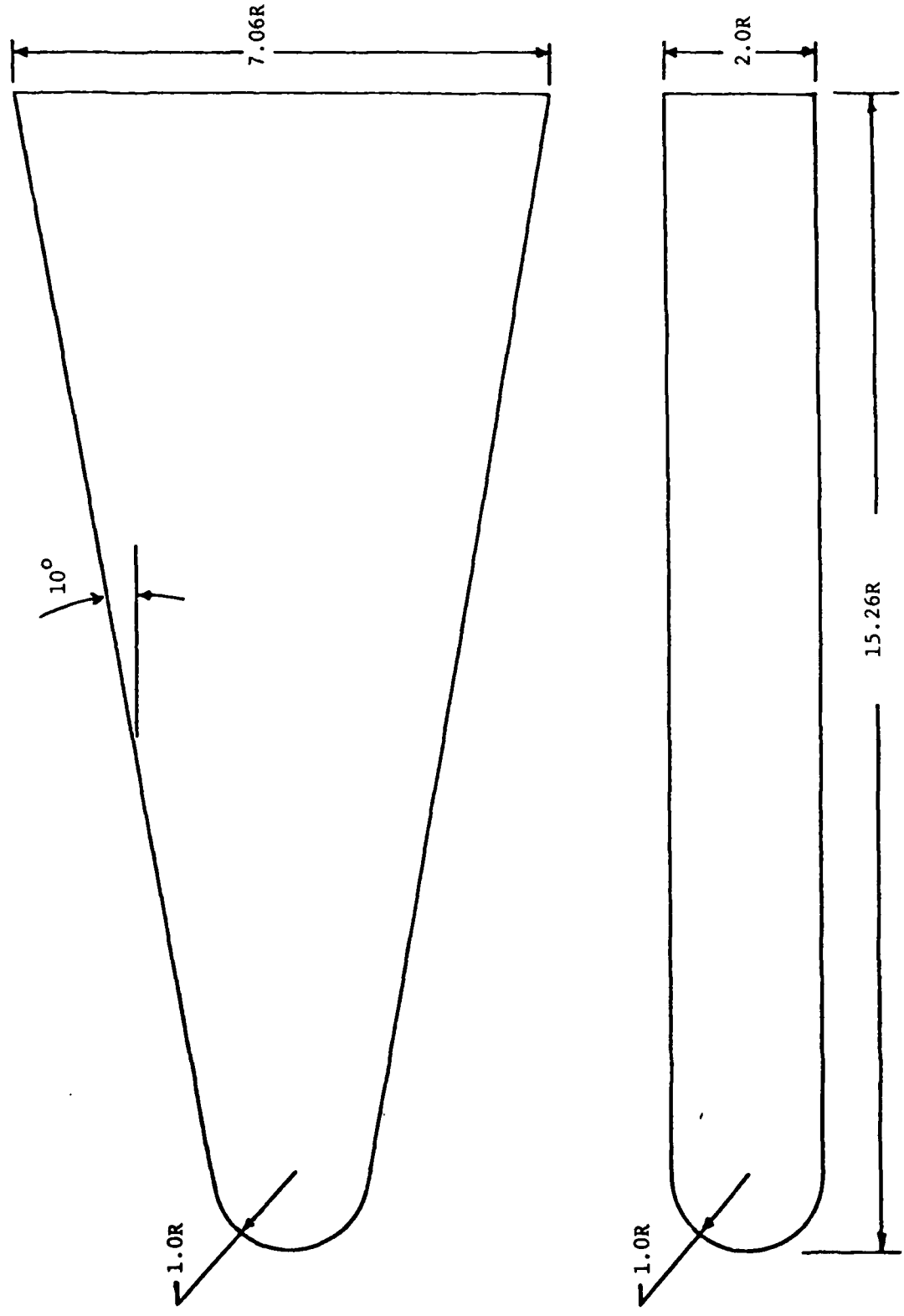

Figure 2. Slab Delta Wing

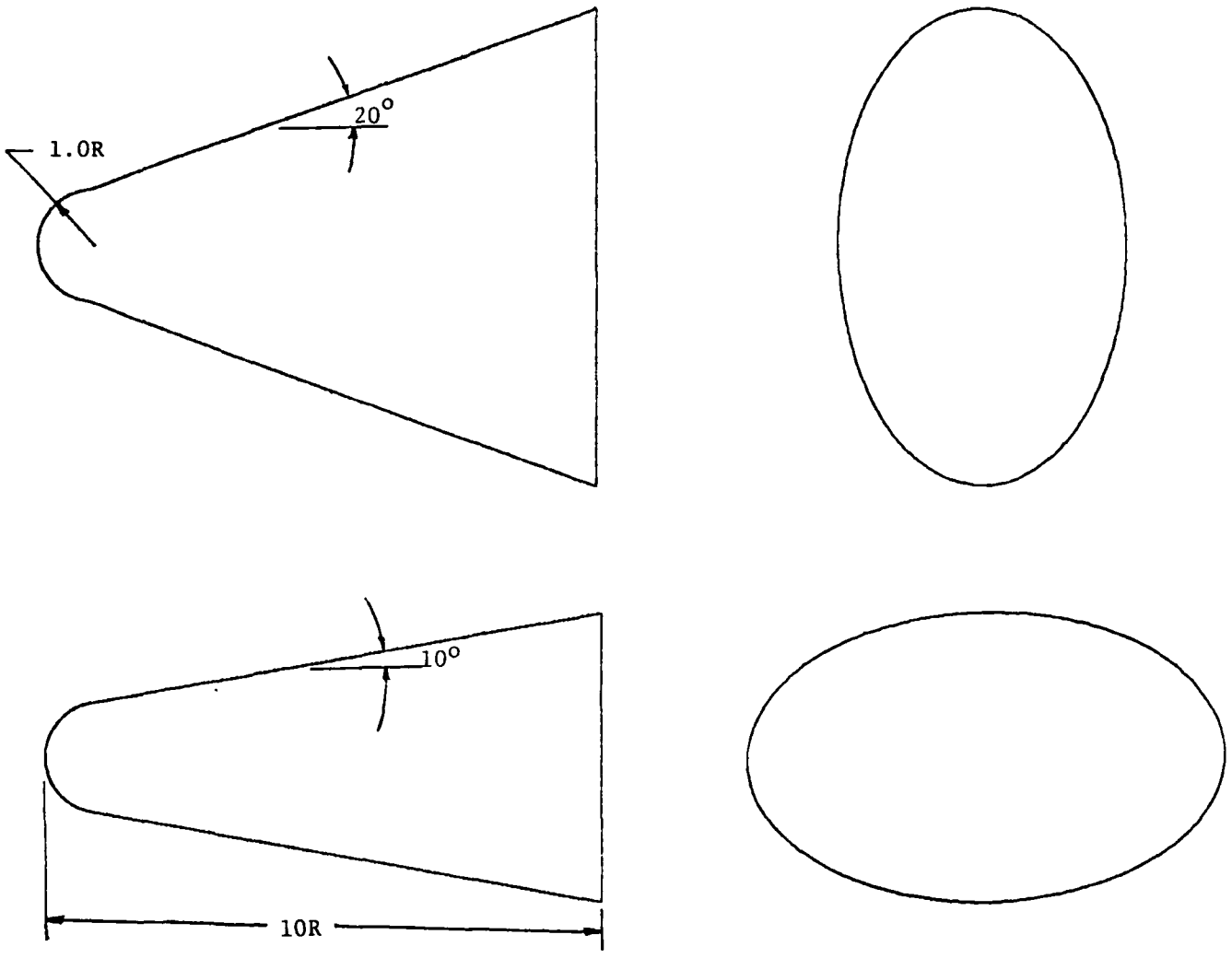

Figure 3. Blunt Elliptic Cone Geometry

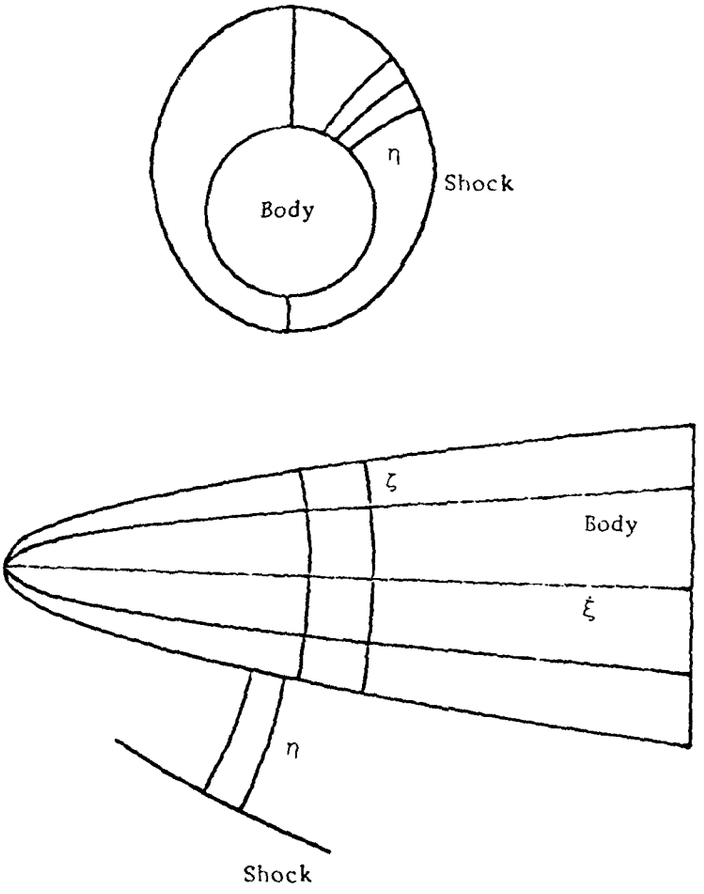

Figure 4. Coordinate System for HYTAC

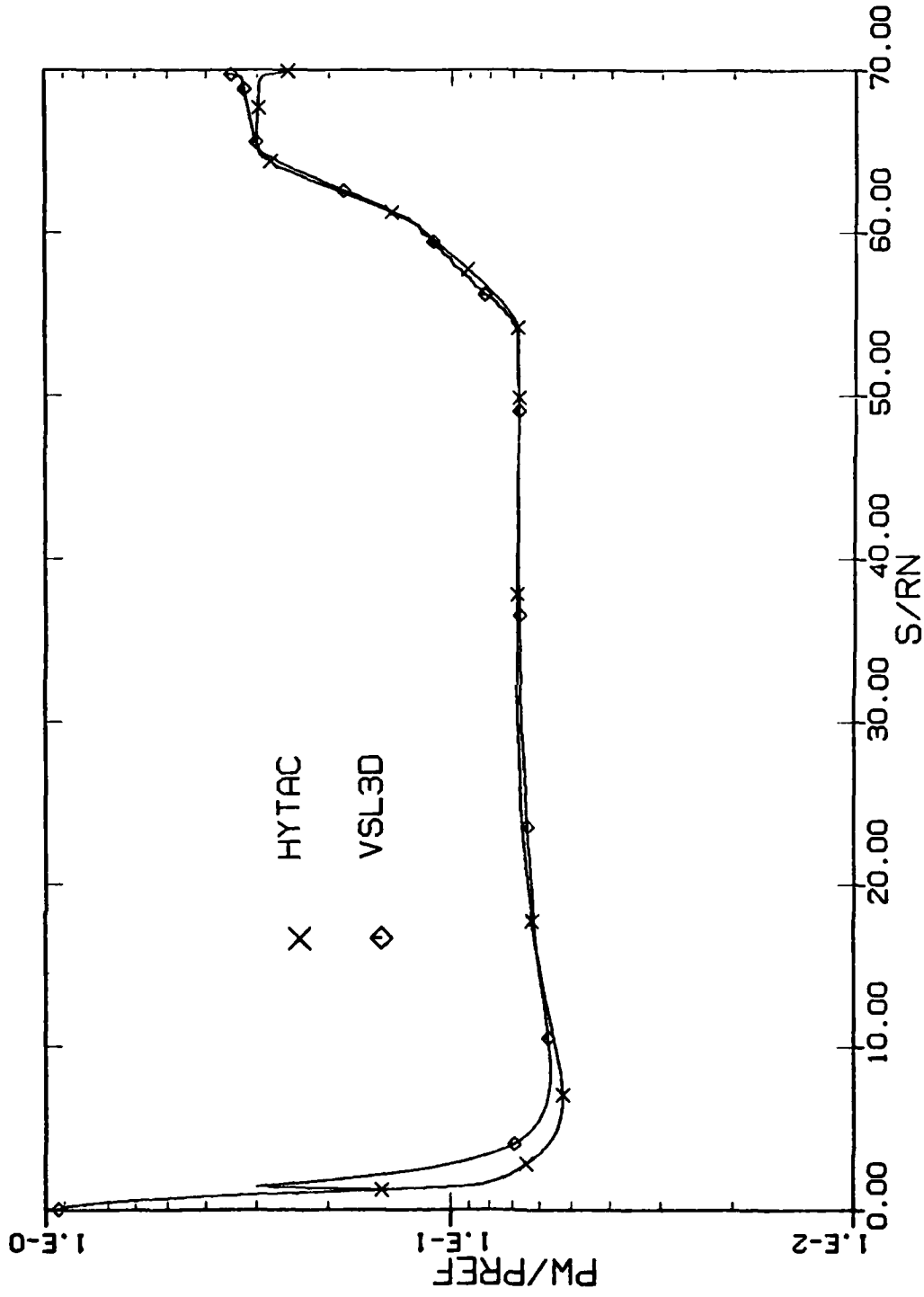

Figure 5. Surface Pressure Distribution for Inlet Geometry at $\alpha = 0$

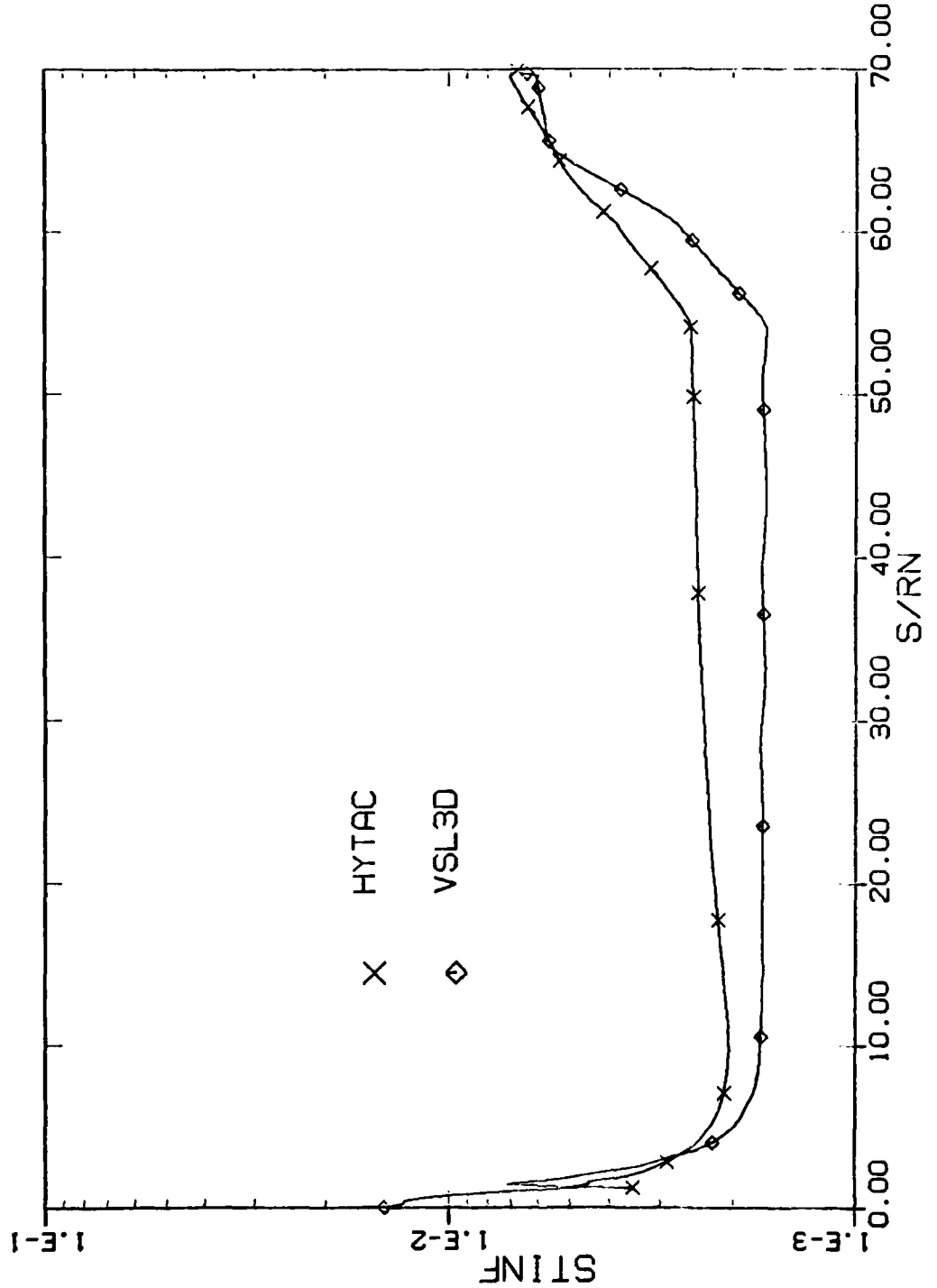

Figure 6. Surface Heat-Transfer Distribution for Inlet Geometry at $\alpha = 0$

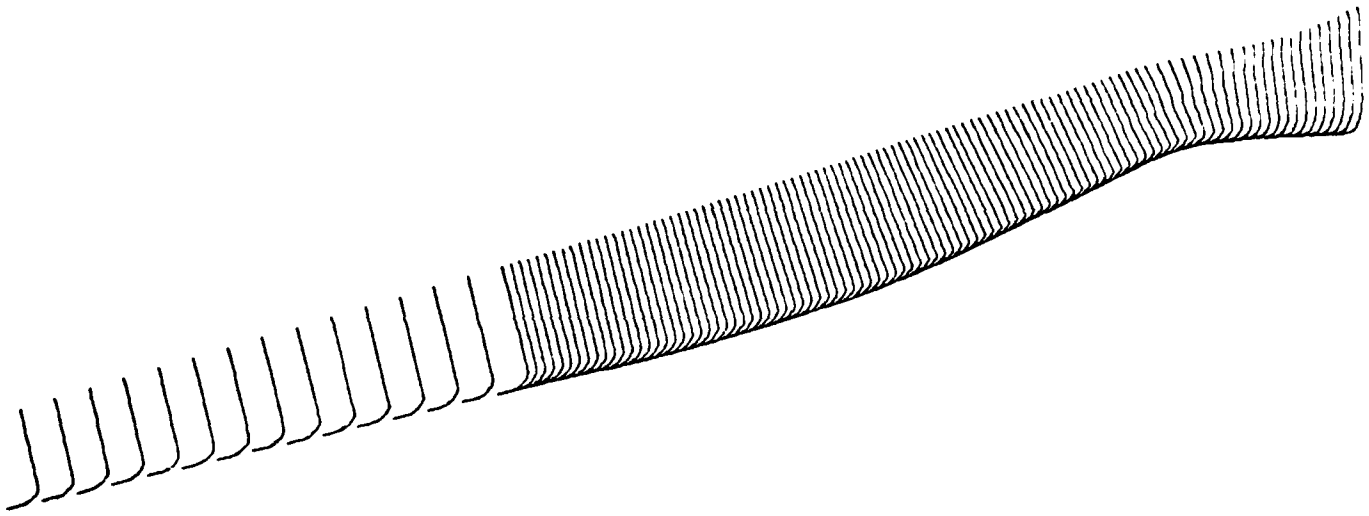

Figure 7. Axial Velocity Profiles for Inlet Geometry at $\alpha = 0$

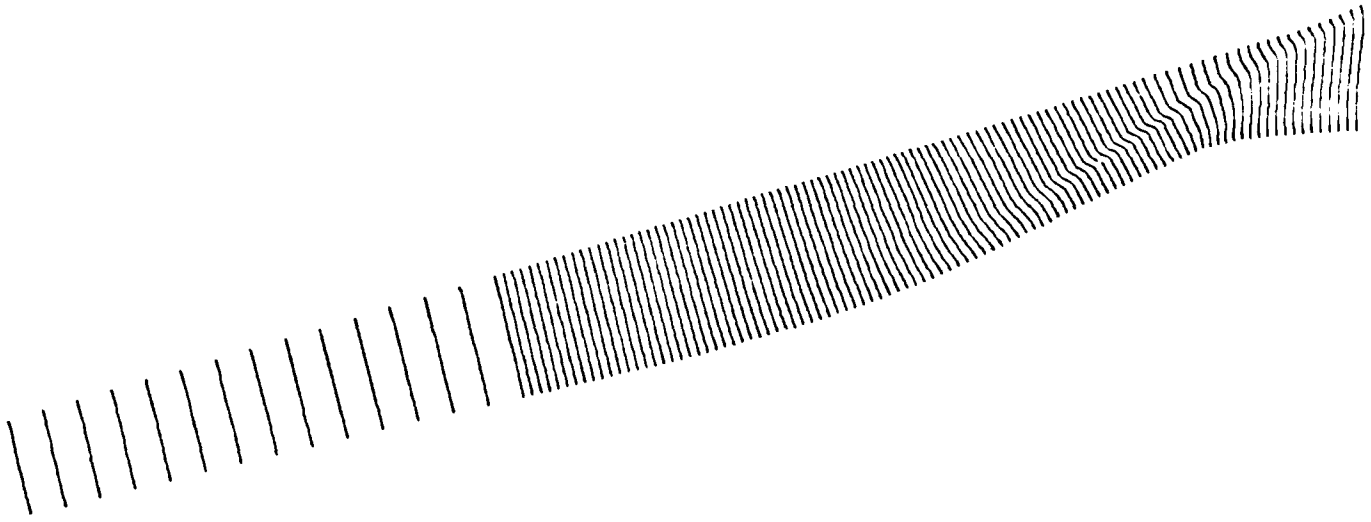

Figure 8. Static Pressure Profiles for Inlet Geometry at $\alpha = 0$

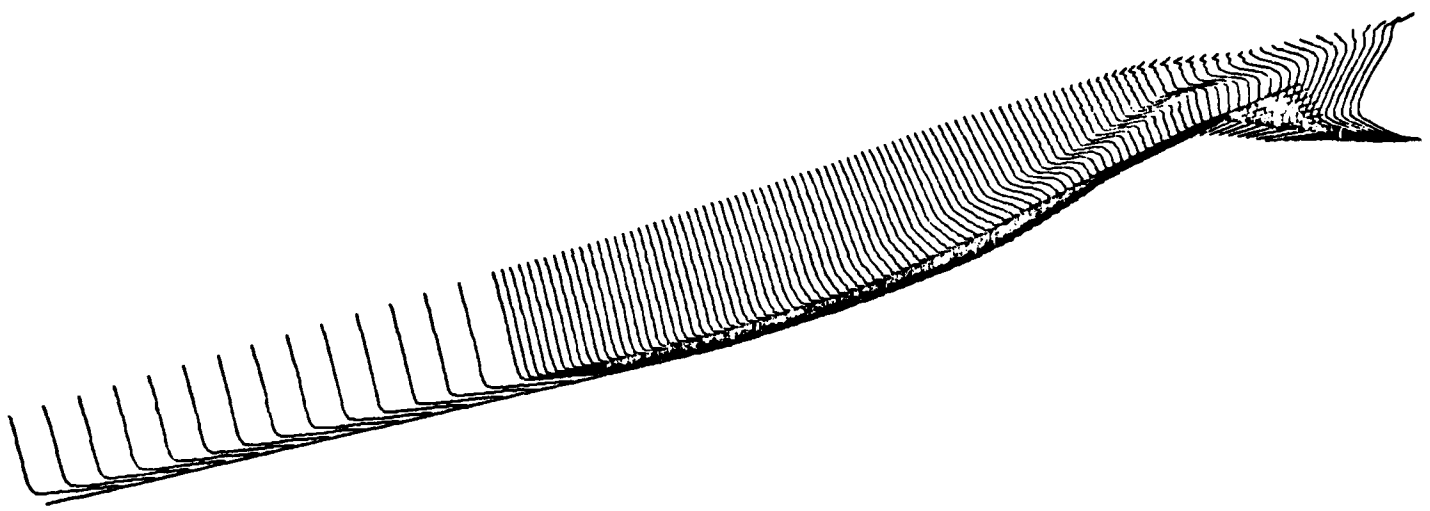

Figure 9. Static Enthalpy Profiles for Inlet Geometry at $\alpha = 0$

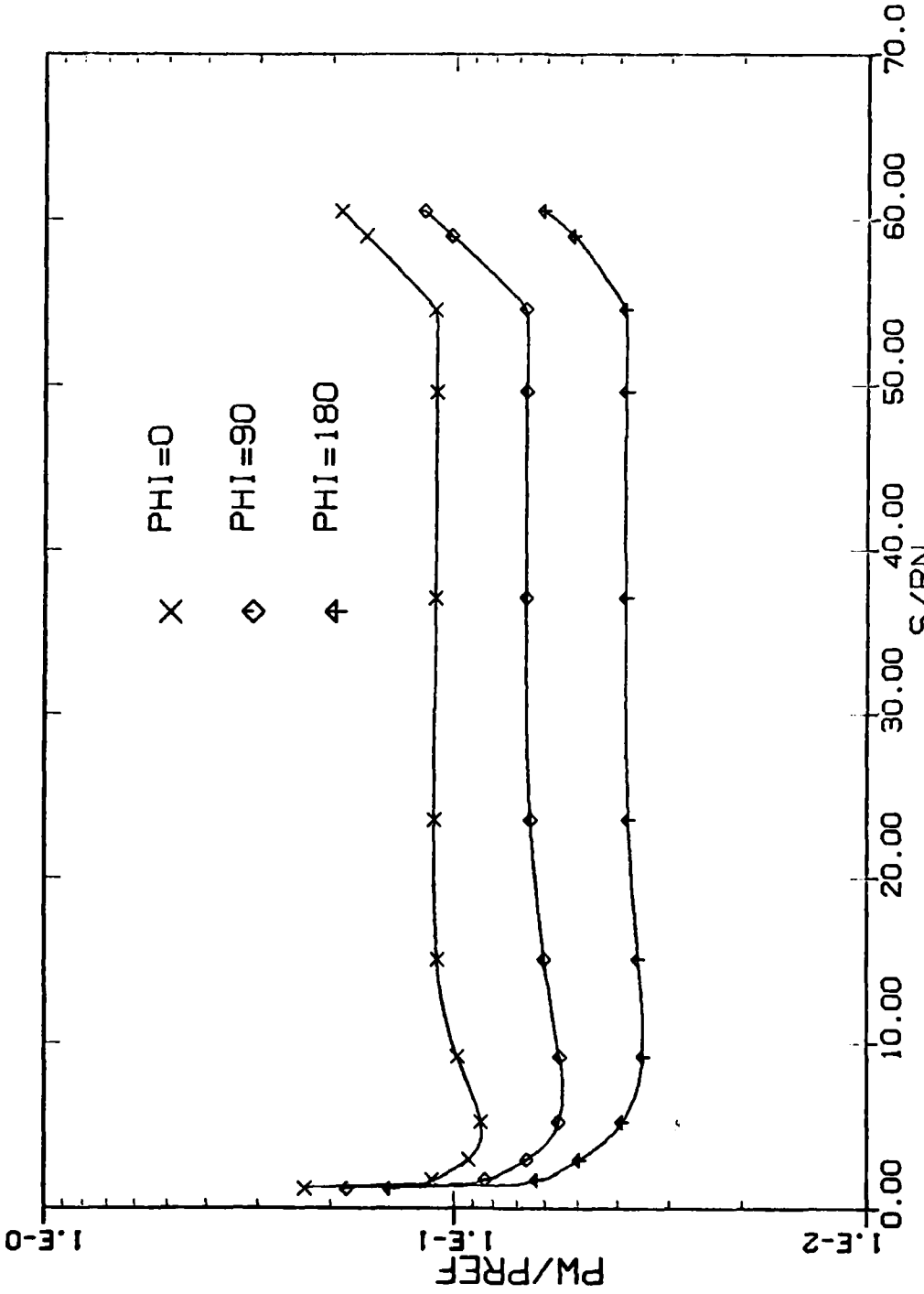

Figure 10. Surface Pressure Distribution for Inlet Geometry at $\alpha = 5^{\circ}$

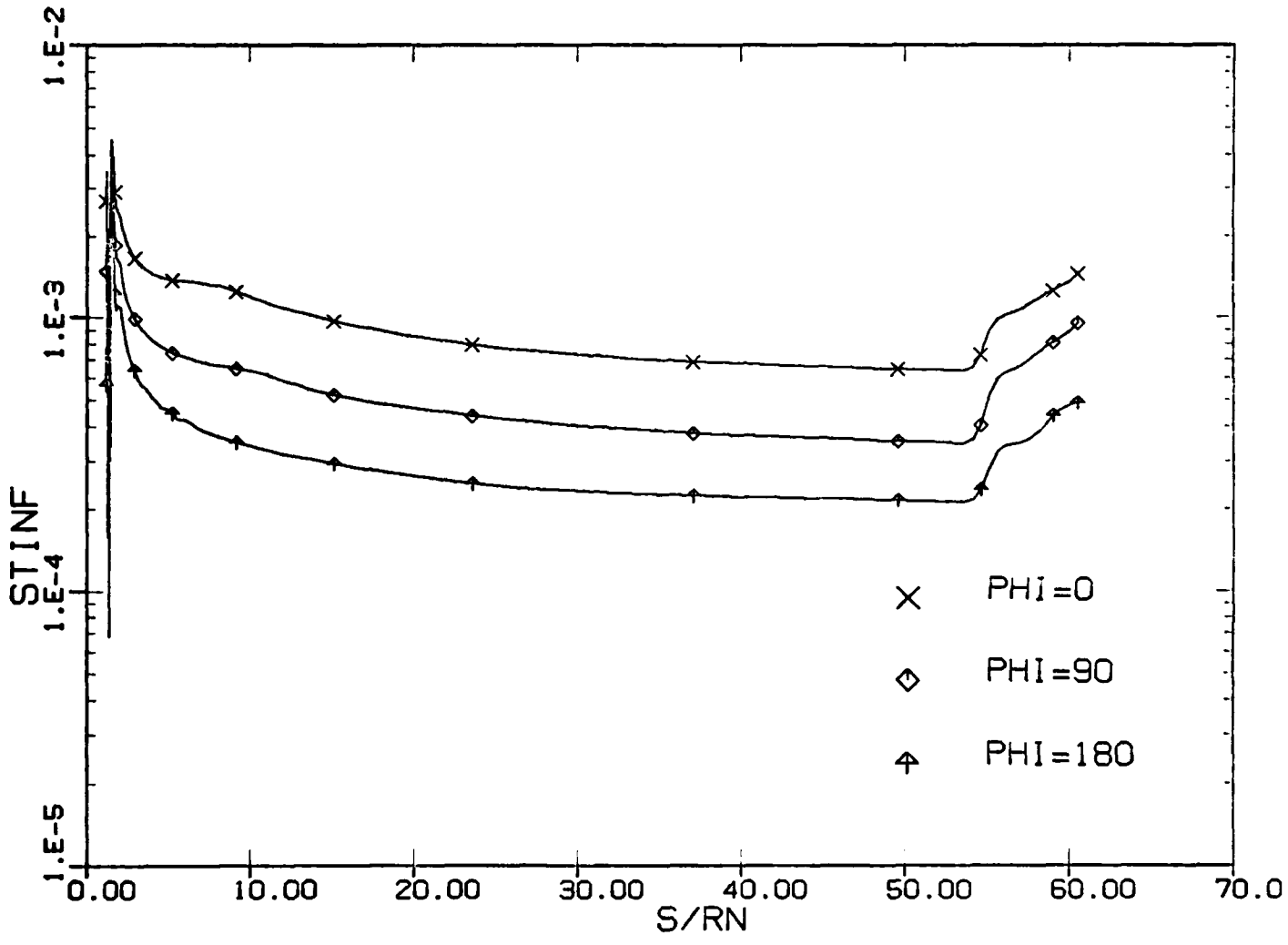

Figure 11. Surface Heat-Transfer Distribution for Inlet Geometry at $\alpha = 5^{\circ}$

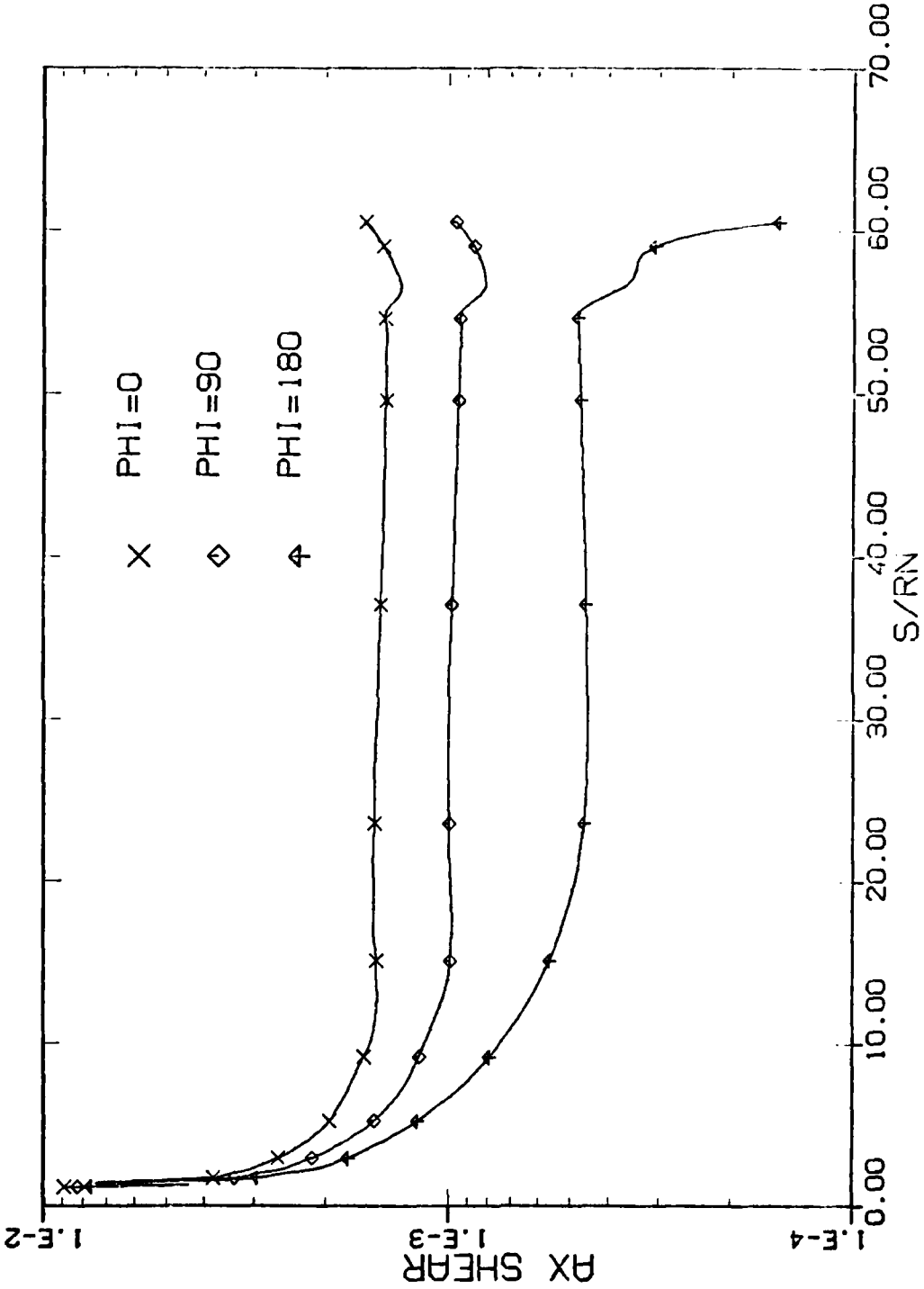

Figure 12. Axial Shear-Force Distribution for Inlet Geometry at $\alpha = 5^{\circ}$

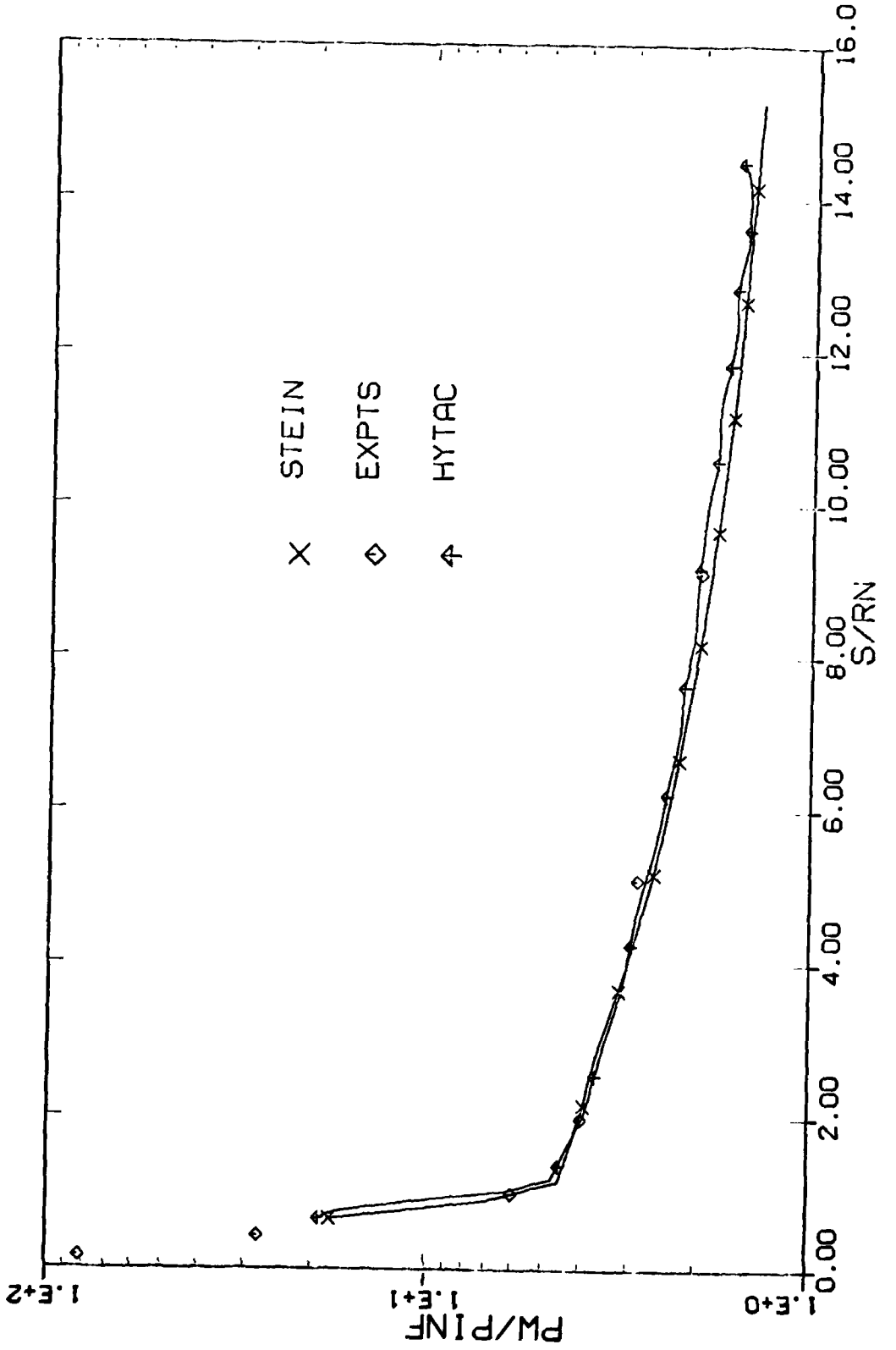

Figure 13. Surface Pressure Distribution for Slab Delta Wing at $\alpha = 0$ and $\zeta = 0$

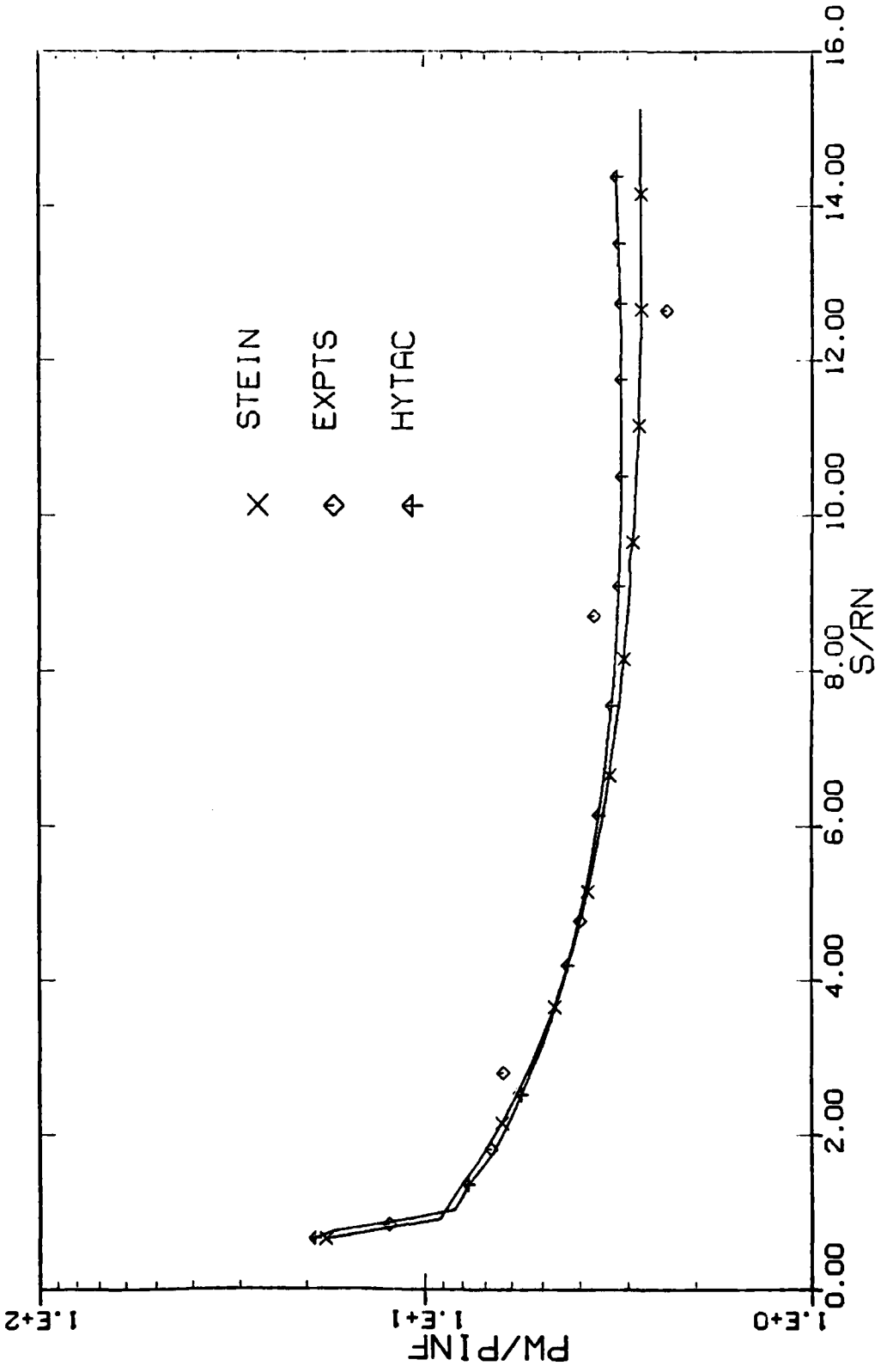

Figure 14. Surface Pressure Distribution for Slab Delta Wing at $\alpha = 0$ and $\zeta = 90$ deg

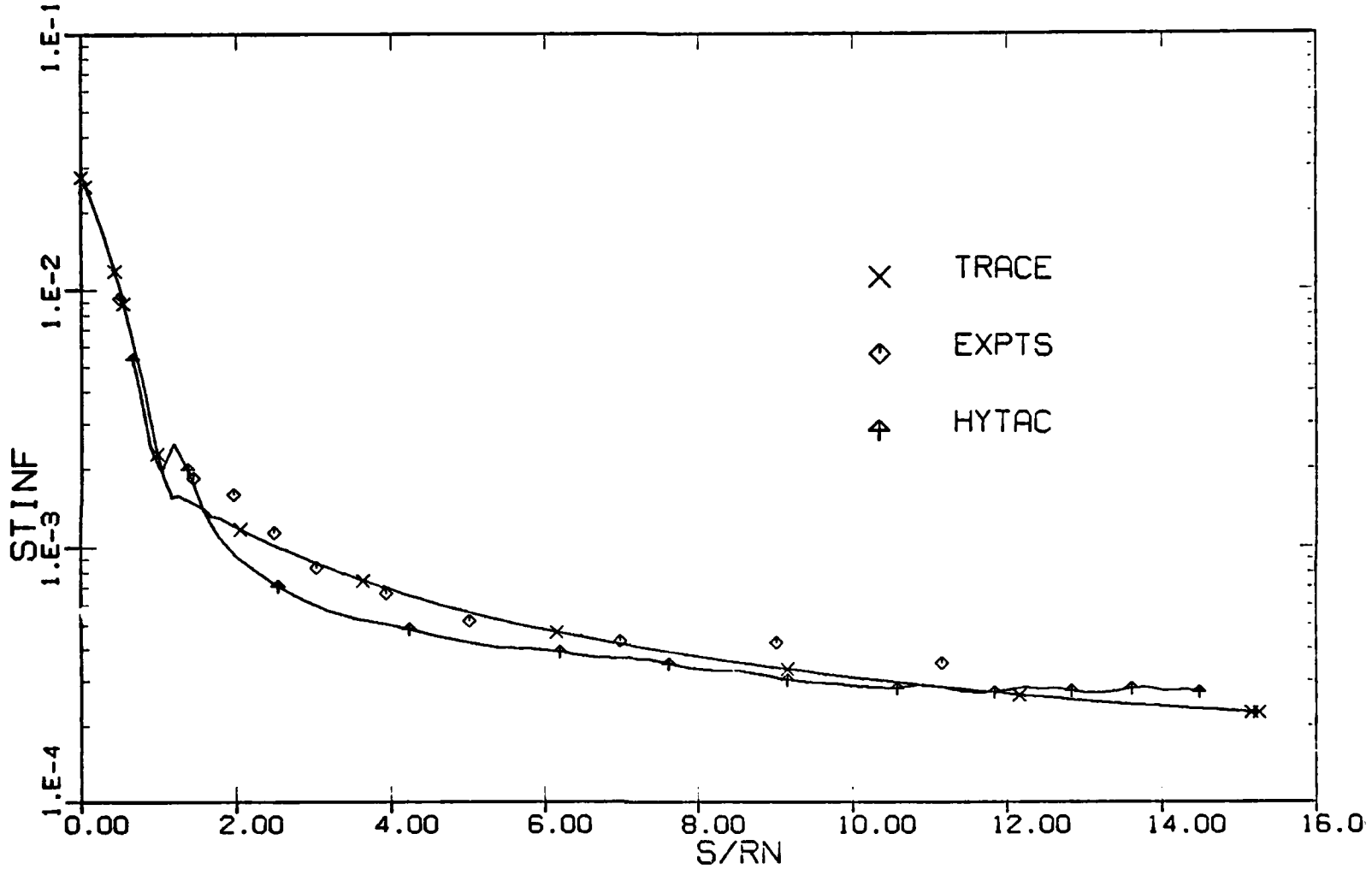

98-II

Figure 15. Surface Heat-Transfer Distribution for Slab Delta Wing at $\alpha = 0$ and $\zeta = 0$ deg

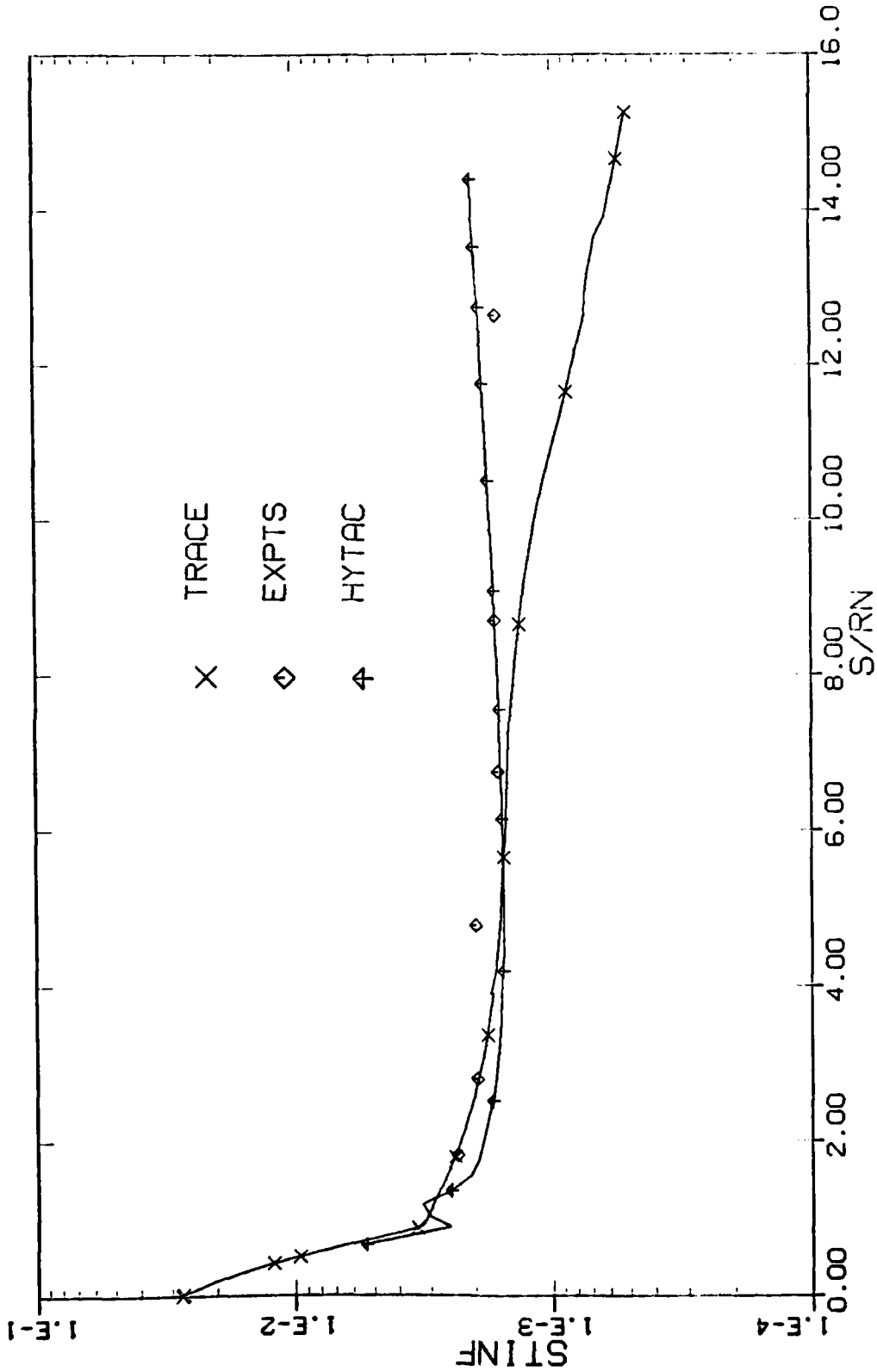

Figure 16. Surface Heat-Transfer Distribution for Slab Delta Wing at $\alpha = 0$ and $\zeta = 90$ deg

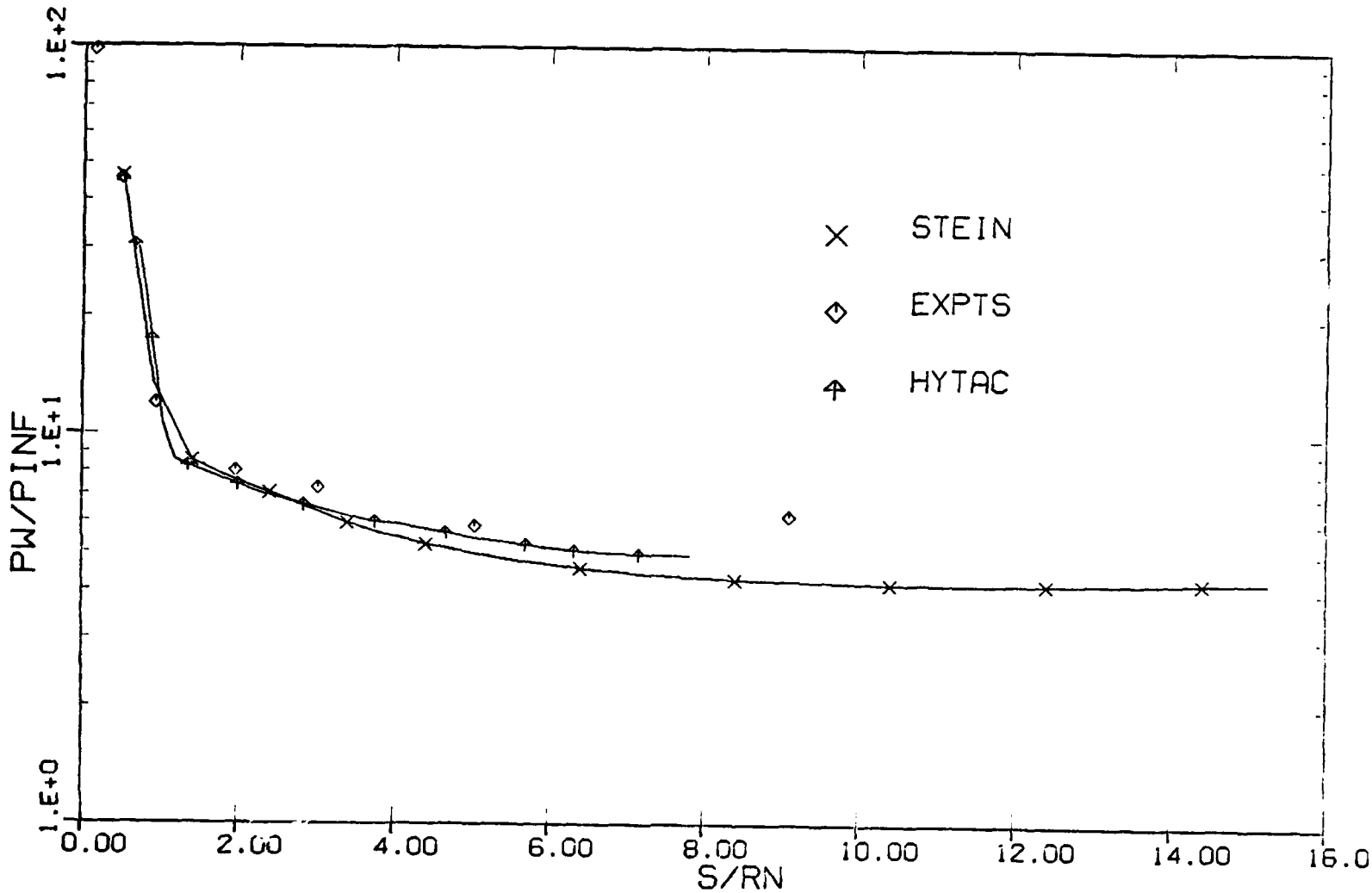

Figure 17. Surface Pressure Distribution for Slab Delta Wing at α = 10 and ζ = 0 deg

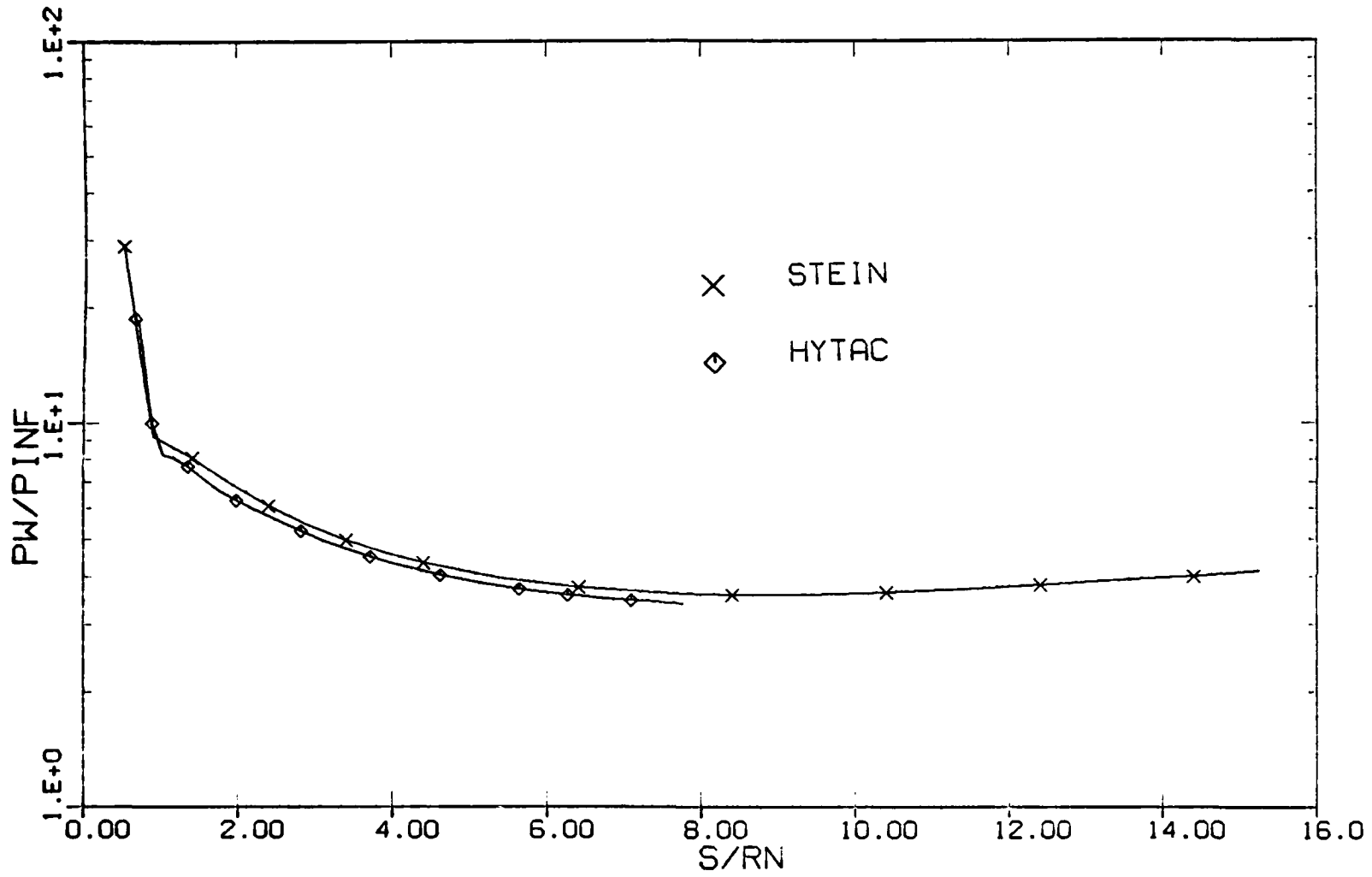

Figure 18. Surface Pressure Distribution for Slab Delta Wing at α = 10 and ζ = 90 deg

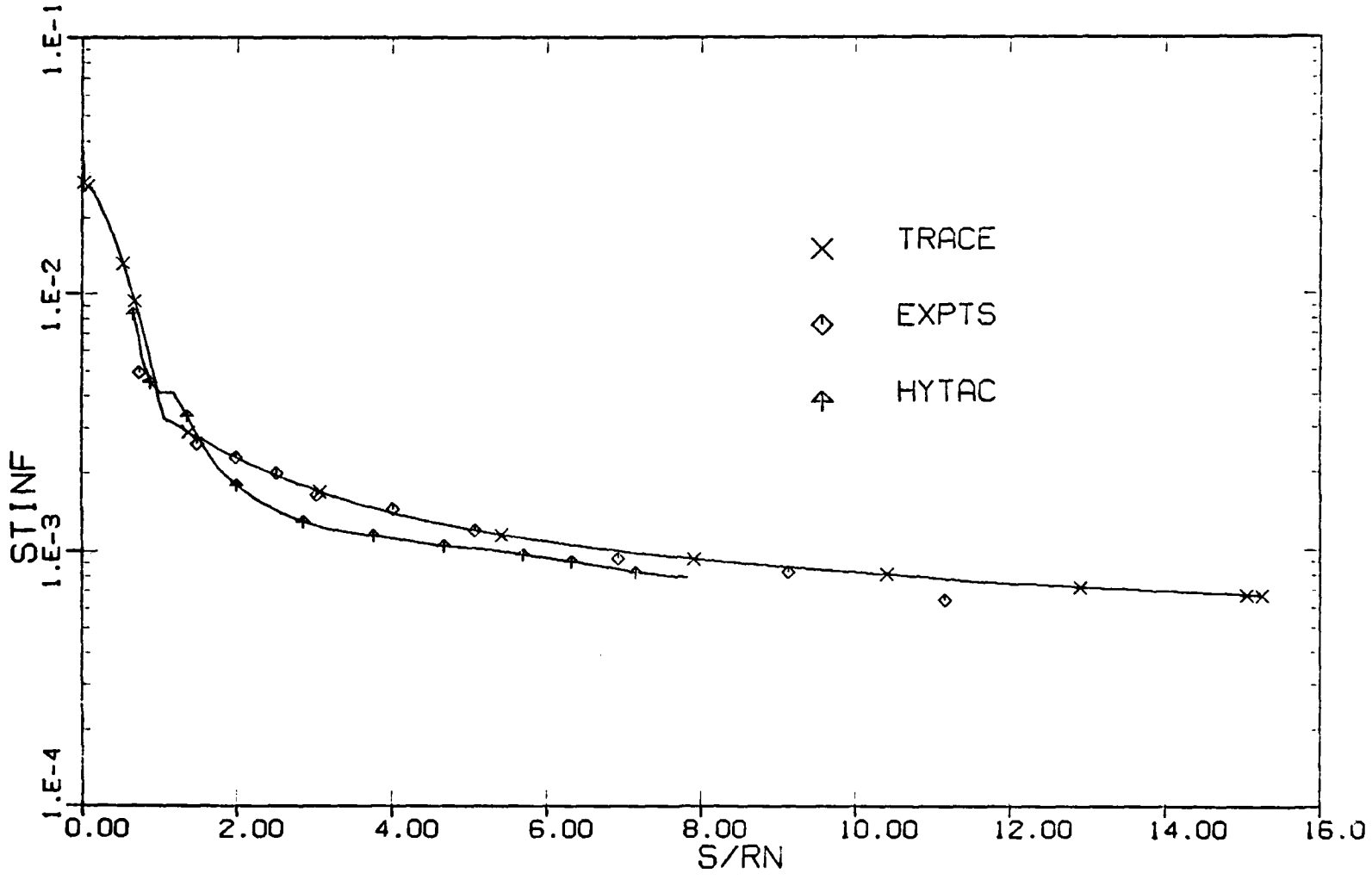

06-11

Figure 19. Surface Heat-Transfer Distribution for Slab Delta Wing at α = 10 and ζ = 0 deg

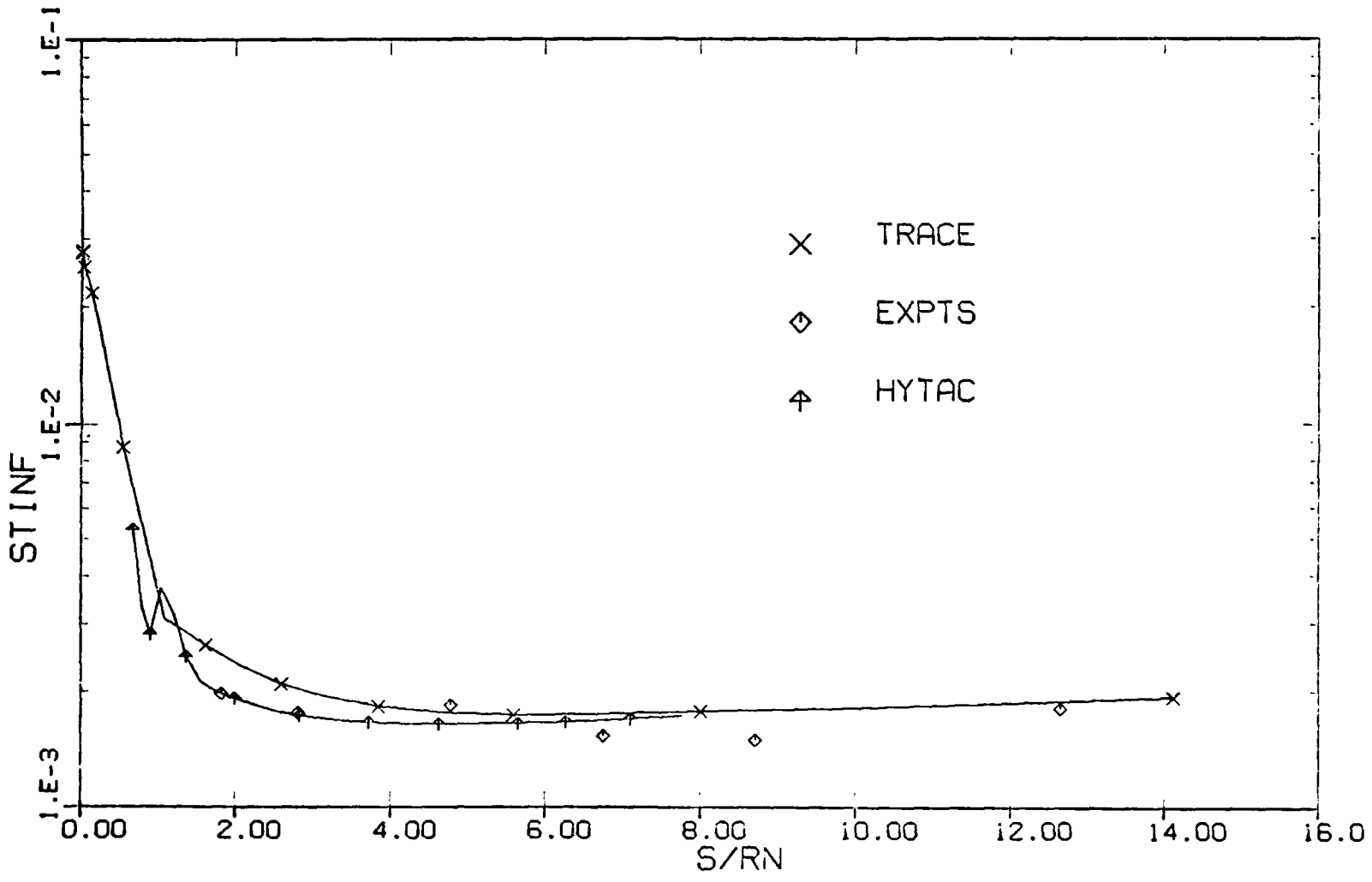

Figure 20. Surface Heat-Transfer Distribution for Slab Delta Wing at α = 10 and ζ = 90 deg

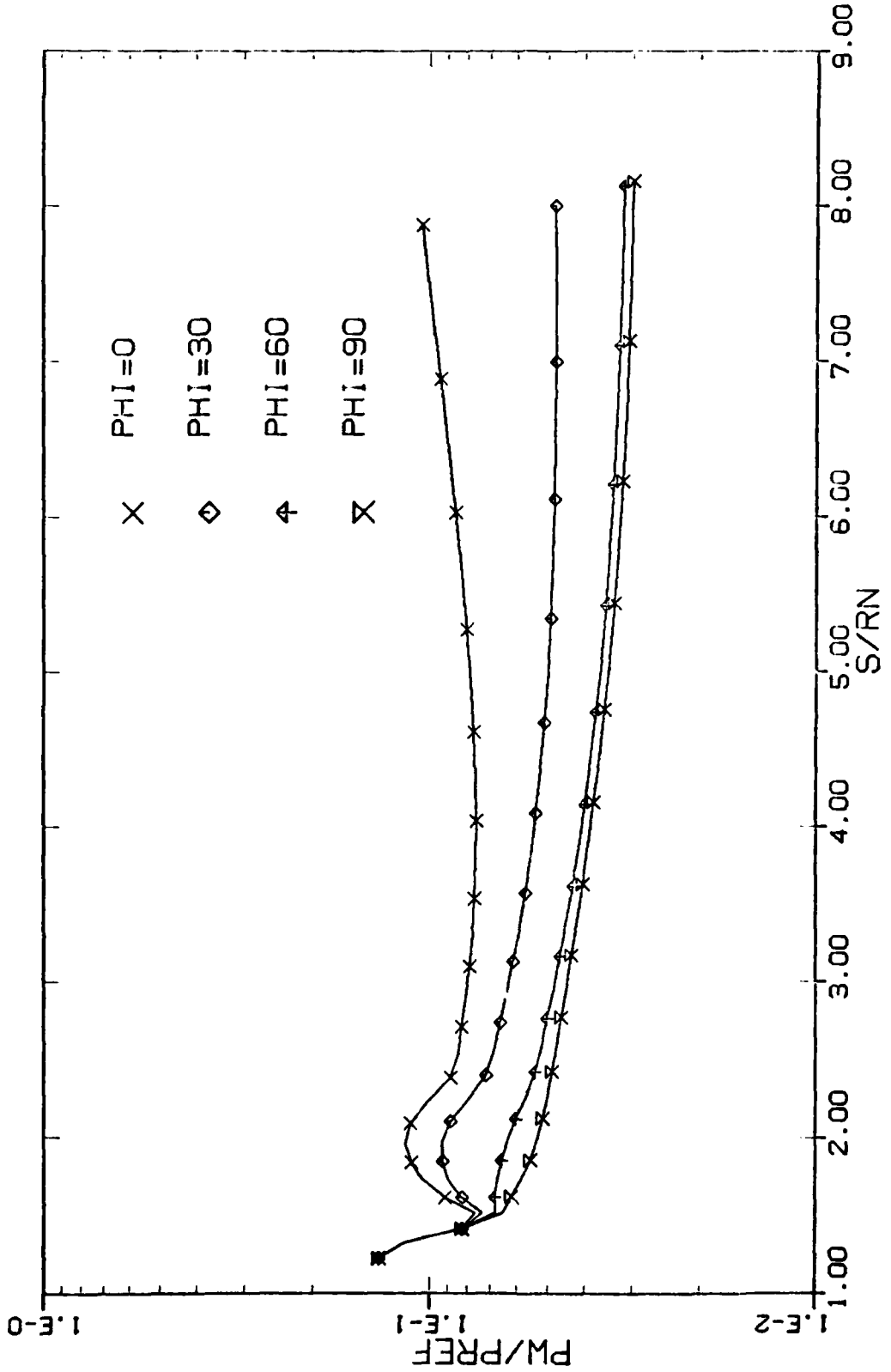

Figure 21. Surface Pressure Distribution for Elliptic Body at $\alpha = 0$

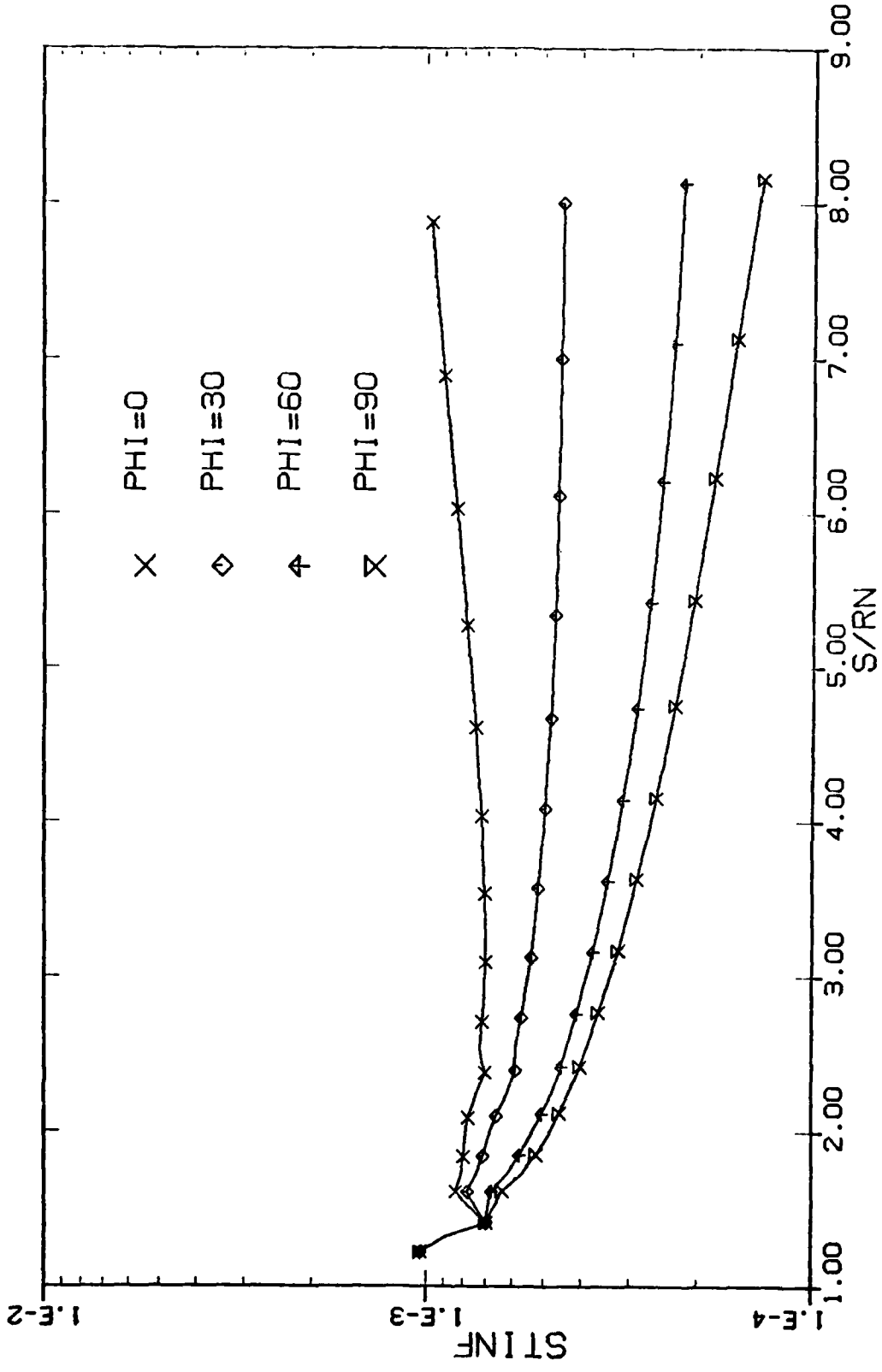

Figure 22. Surface Heat-Transfer Distribution for Elliptic Body at $\alpha = 0$

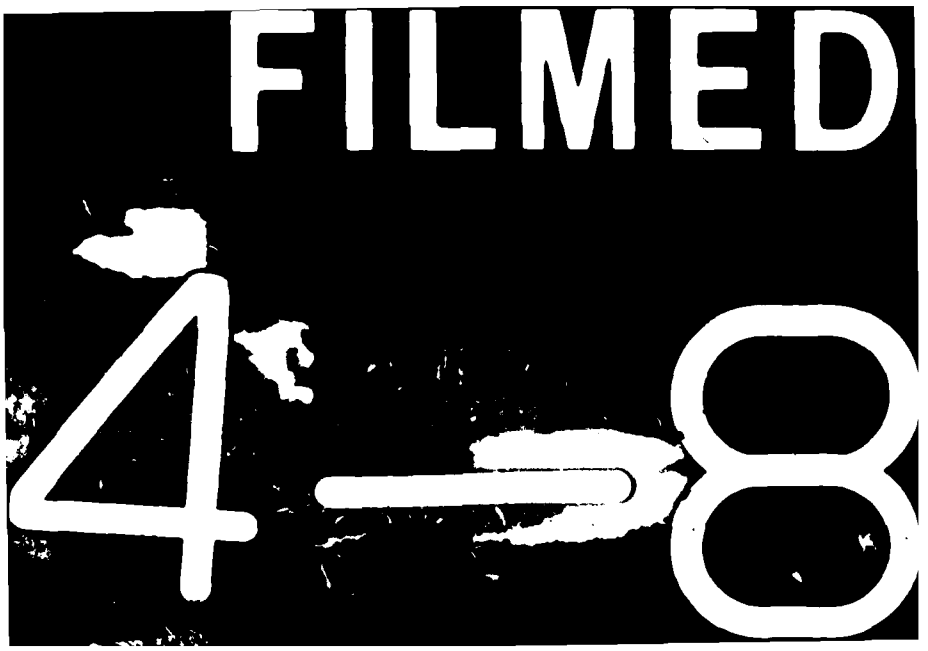
FILMED
4-8